Composites Communications 64 (2026) 102823

Contents lists available at ScienceDirect

Composites Communications

journal homepage: www.elsevier.com/locate/coco

Interlayer engineering of shape memory phthalonitrile based composites via PTFE decoupling and aerogel functionalization

Rongxiang Hu [a], Fenghua Zhang [a,*], Yanju Liu [b], Jinsong Leng [a,**]

[a] Centre for Composite Materials and Structures, Harbin Institute of Technology (HIT), Harbin, 150080, People's Republic of China
[b] Department of Astronautical Science and Mechanics, Harbin Institute of Technology (HIT), Harbin, 150001, People's Republic of China

ARTICLE INFO

Keywords:
Shape memory polymer composites
Sandwich structure
Thermal protection

ABSTRACT

Shape memory polymers (SMPs) are stimuli-responsive smart materials with great potential for engineering applications. Fiber reinforced SMP composites (SMPCs) are widely used to enhance mechanical properties while retaining shape memory performance. However, although multilayer fiber fabrics reinforced SMPC laminates offer higher mechanical strength, their deformation during shape memory process is often constrained by interfacial restrictions between adjacent plies. In this study, a polytetrafluoroethylene (PTFE) interlayer strategy was developed to decouple adjacent SMPC plies, and PTFE interlayered, carbon fiber reinforced shape memory phthalonitrile laminate composites (SMPN-LC) were fabricated. Mechanical tests indicates that, at an interlaminar bonding area of 20%, SMPN-LC exhibits a tensile strength of 307 MPa and a flexural strength of 426 MPa. At the same bonding area, as the length-width ratio decreases from 6:1 to 2:1, the flexural strain of SMPN-LC increases from 1.8% to 2.9%, which is attributed to an increased length of the PTFE induced interlaminar decoupling region. SMPN-LC exhibits layer-wise shape memory behavior and can be deformed into a temporary anchor-hook structure capable of hanging a 500 g weight. By incorporating shape memory phthalonitrile aerogel (SMPNA) into SMPN-LC to obtain SMPN-LAC, the thermal conductivity decreases to 104 mW/m·K and provided good thermal insulation performance. In the compressed temporary shape, the SMPNA interlayers within SMPN-LAC recovers gradually to form layer-by-layer thermal barrier, maintaining the opposite-side temperature at around 300 °C after 600 s of butane flame exposure. This interlayer strategy endows SMPN-LAC with good thermal insulation with shape memory performance, broadening the application potential of SMPCs.

1. Introduction

Shape memory polymers (SMPs) are a class of smart materials that can recover from a temporary shape to their original shape in response to external stimuli such as heat, light, and electric fields [1–5]. Benefiting from the low density, large reversible strain, and facile processing, SMPs have attracted considerable interest across soft robotics, biomedical engineering, aerospace, and other emerging fields [6–12]. However, pristine SMPs generally suffer from low mechanical strength and limited recovery force, which restricts their applications.

Incorporating reinforcing phases into SMPs to fabricate SMP composites (SMPCs) is an effective strategy to enhance their mechanical properties. The reinforcements such as short fibers, continuous fibers/fabrics, and particulate fillers allow SMPCs to retain shape memory properties and broaden their functional applications [13–17]. Among various reinforcement materials, carbon fiber (CF) is widely employed in advanced SMPCs due to its high specific strength, high specific modulus, and excellent thermal resistance [18–20]. CF reinforced SMPCs can provide high mechanical strength at low mass, making them attractive for lightweight actuation systems. Zeng et al. [21] developed a CF reinforced SMPC laminate based on shape memory cyanate, which exhibits excellent environmental stability and bearing capacity, enabling its application as a space-deployable locking and release device. Li et al. [22] reinforced a bismaleimide-based SMPC with CF, enhancing its strength and stiffness and enabling a retractable claw capable of grasping loads 29.8 times its own weight. These studies suggests that the great potential of SMPCs for advanced applications.

In CF reinforced composites, unidirectional CF and twill-woven CF

* Corresponding author.
** Corresponding author.
E-mail addresses: fhzhang_hit@163.com (F. Zhang), lengjs@hit.edu.cn (J. Leng).

https://doi.org/10.1016/j.coco.2026.102823
Received 10 March 2026; Received in revised form 15 April 2026; Accepted 15 April 2026
Available online 17 April 2026

fabrics are widely used reinforcements [23–26]. Owing to the interlaced warp and weft architecture, twill fabrics generally offer more balanced in-plane properties, and multilayer fabric layups are commonly adopted in engineering to achieve more uniform performance. In the composites based on conventional resins, multilayer fabric laminates greatly improve the mechanical performance. However, in SMPC, multilayer fabric laminates often restrict its deformation during the shape memory process due to interfacial constraints between adjacent plies. In addition, CF reinforced composites typically exhibit a single shape memory mode, which limits their use in other functional applications.

In this work, a polytetrafluoroethylene (PTFE) interlayer strategy was developed to decouple adjacent SMPC plies. CF reinforced shape memory phthalonitrile composites (SMPNC) were fabricated, and PTFE interlayers were introduced to obtain the laminate composite SMPN-LC. The influence of interlaminar bonding area on the mechanical properties of SMPN-LC was investigated. As the interlaminar bonding length decreases, the regions of PTFE-induced decoupling increases, leading to higher flexural strain. With interlaminar decoupling, SMPN-LC exhibits layer-wise shape memory behavior, thereby enhancing deformation adaptability of SMPC. Furthermore, shape memory phthalonitrile aerogel (SMPNA) was incorporated into SMPN-LC to preparate SMPN-LAC, reducing the thermal conductivity of the composite and enabling good thermal insulation performance. The shape memory behavior of SMPNA enables SMPN-LAC to recover gradually from a compressed temporary shape and form layer-by-layer thermal barrier under butane flame exposure, thereby exhibiting good thermal protection performance. This study provides new insights into functional applications of advanced SMPCs.

2. Material and methods

2.1. Materials

The phthalonitrile monomer, end-capping reagent, and SMPNA were obtained in our laboratory following the procedures reported in our previous studies [27,28]. N, N-dimethylformamide (DMF) and bis [4-(3-aminophenoxy)phenyl] sulfone (m-BAPS) were purchased from Aladdin Co. T300-type twill carbon fibric was from Toray Industries. PTFE-coated fiberglass fabric (Teflon fabric) was purchased from Zhendang Composite Materials Co.

2.2. Preparation of the composites

Preparation of SMPNC prepregs. The monomer containing aromatic ether ketone chains, the biphenyl based end-capping reagent, and the curing agent (m-BAPS) were melted and mixed at 200 °C for 5 min, after which the SMPN prepolymer was cooled to room temperature for subsequent use. The prepolymer was dissolved in DMF to prepare a 50 wt% solution and used to impregnate the CF fabric, the specific preparation procedure is shown in Fig. 1a. After stepwise heating at 100 °C for 1 h, 150 °C for 30 min, and 200 °C for 15 min, the impregnated fabric was converted into SMPNC prepreg with a resin solid content of approximately 50%.

Preparation of SMPNC. The SMPNC prepregs were stacked and clamped in a flat mold and then placed in an oven for curing according to the following schedule: 220 °C for 2 h, 260 °C for 4 h, 280 °C for 4 h, 300 °C for 4 h, 325 °C for 4 h, and 350 °C for 4 h. Composites with different CF stacking sequences were prepared by changing the fabrics orientation, including ±45° layups (±45), 0°/90° layups (0/90), and interlayer-alternating ±45° and 0°/90° layups (IA).

Preparation of SMPN-LC. The PTFE fabric was laser-cut to form a central cutout and inserted between adjacent SMPNC prepreg plies. The cutout region was filled with SMPN prepolymer. The laminate was then clamped and cured in an oven to obtain SMPN-LC. Conventional SMPCs are typically fabricated as thin sheets to achieve large deformations by reducing bending stiffness and interlaminar constraints. The introduction of PTFE enables interlaminar decoupling, effectively reducing constraints between adjacent plies and thereby enhancing the overall

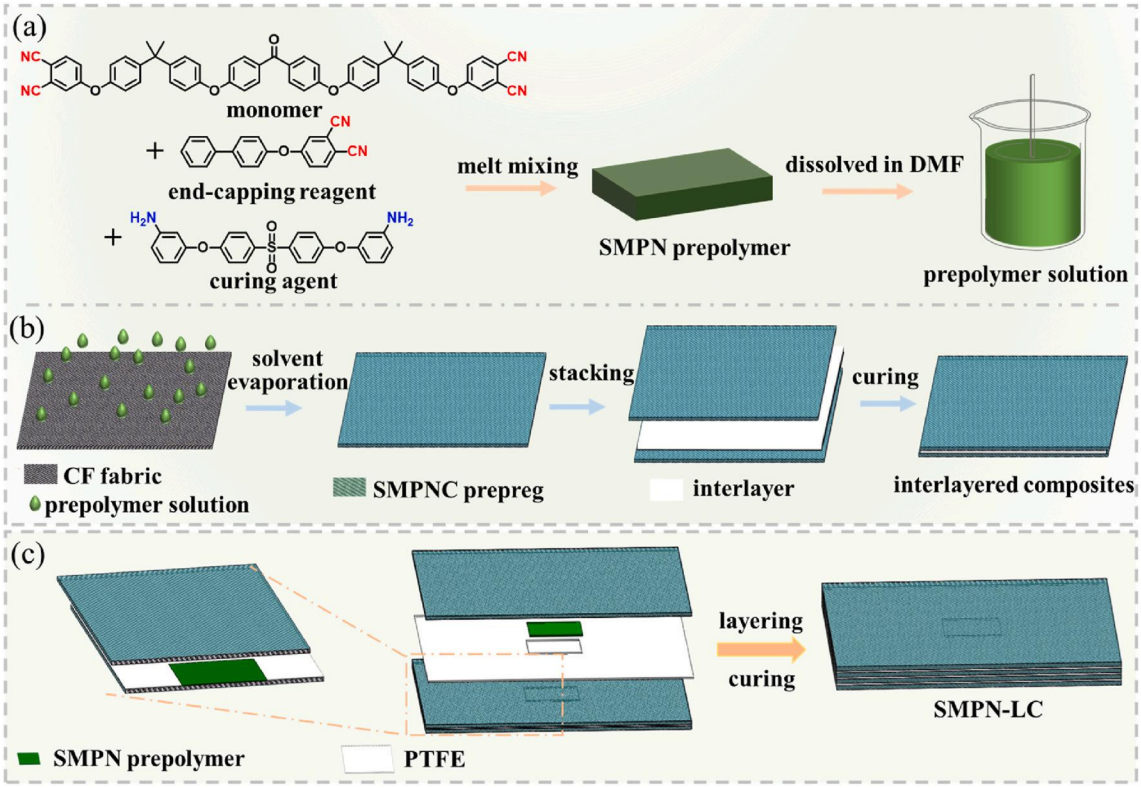

Fig. 1. Schematic of the preparation process for the interlayered composites: (a) preparation of SMPN prepolymer solution, (b) fabrication of interlayered composites. (c) Schematic illustration of the SMPN-LC interlaminar structure.

deformation capability of the structure. Thick SMPN-LC components can be fabricated by alternately stacking SMPNC prepreg plies and PTFE layers, with the thickness increasing as the number of layers increases.

Preparation of SMPN-LAC. The thickness of the SMPNA was controlled to approximately 3 mm, and it was processed to the same sizes as the SMPNC prepreg. SMPN prepolymer and 2 wt% carbon nanotubes (CNTs) were blended together in a high-speed crusher. The mixture was then heated to melt completely, yielding a prepolymer/CNT blend. The molten blend was subsequently melt-rolled several times into thin sheets, which were molded to match the dimensions of the cutout region of PTFE. SMPNA, with a thermal conductivity of around 40 mW/m·K at 25 °C, was used as the core layer and was sandwiched between two prepreg/PTFE plies to form a sandwich structure. The stacked composite was then placed in a flat mold and cured according to the prescribed schedule to obtain the SMPN-LAC.

2.3. Characterization

Scanning electron microscope (SEM) was used to observe the micro morphology performed on TESCAN AMBER. Dynamic mechanical analysis (DMA) was performed to investigate the dynamic mechanical properties of obtained resins using the DMA Q800 (TA Co., America) recorded in multi-frequency strain mode at a constant frequency of 1 Hz with a heating rate of 5 °C min^{-1} from 25 °C to 400 °C. Mechanical properties were evaluated using an Instron 5500R electronic universal testing machine. The tensile tests were performed on specimens with dimensions of 250 mm × 25 mm × 1.5 mm at a crosshead speed of 2 mm/min. The flexural tests were carried out in a three-point bending configuration using specimens of 10 mm × 12 mm × 1.5 mm, with a support span of 64 mm and a crosshead speed of 2 mm/min.

3. Result and discussion

3.1. The interface characterization of SMPN-LC

Fig. 1b presents the preparation procedure for the interlayered composites, and Fig. 1c shows the schematic illustration of the interlayer structure of SMPN-LC. The SMPN prepolymer that filled the cutout regions of the PTFE plies cured upon heating, thereby bonding adjacent SMPNC plies into an integrated laminate. The centrally bonded region ensures SMPN-LC structural integrity and provides strength support, whereas the PTFE covered regions form decoupling zones with reduced interlaminar constraints due to the low surface energy of PTFE, enabling large bending deformation via interfacial slip.

The bending deformation behavior of the composite was simulated using a simplified model in three-point bending test, with simulation details presented in Supporting Information Fig. 2a shows the simulated cloud diagram for the conventional SMPC reinforced with two CF fibric layers. Due to the constraints at the interlayer, as the deflection increases, a higher stress concentration develops in the loading area. With the interlayer of PTFE, Fig. 2b shows that its decoupling effect enables the SMPC layers to bend independently, dispersing concentrated stress between the layers and effectively reducing the bending stress that result from the thickness. Fig. 2c presents the extracted reaction force-displacement curves at the loading nose. At a displacement of 2 mm, the reaction force of the SMPC is 54.5 N, while that of the PTFE interlayered SMPC is 25.7 N, corresponding to a reduction of 52.8%. These simulation results demonstrate that the decoupling of the PTFE interlayer can effectively disperse the concentrated stress in the SMPC interlayer, thereby facilitating the deformation of the composite.

A shape memory deformation experiment was conducted to visually demonstrate the decoupling effect of the PTFE interlayer. Fig. S1 presents photographs of the temporary shapes of a conventional SMPNC laminate and a PTFE interlayered SMPN-LC. Due to interlayer constraints, the deformation of the SMPNC laminate is relatively difficult and limited, and internal wrinkling even occurs under in-plane bending compression. In contrast, SMPN-LC exhibits greater deformability and maintains a smooth in-plane surface due to the decoupling of the PTFE interlayer, which disperses stress concentrations during the deformation process.

Fig. 3a shows that the decoupling zone can deform under external force at room temperature. Fig. 3b shows a side view of the interlaminar bonding region in SMPN-LC, where the boundary between the PTFE and SMPNC plies is clearly visible. After peeling off the SMPN-LC, the macroscopic morphology of the interfacial bonding region is shown in Fig. 3c. A distinct boundary is observed between the bonded region and the PTFE isolated region. The PTFE interlayer decouples adjacent SMPNC plies, while the SMPN-LC maintains its integrity due to the curing of the filled SMPN. The micromorphology of the bonding regions on both delaminated surfaces was characterized by SEM. Fig. 3d shows exposed carbon fibers on the SMPNC ply surface after peeling, and Fig. 3e reveals grooves left in the resin on the opposite surface caused by fiber pull out. Fig. 3f presents a cross-sectional SEM image of the bonding region, showing that the interfacial resin tightly wraps the fibers, thereby supporting structural integrity and mechanical strength via effective impregnation.

Interlaminar bonded strength plays a critical role in the structural stability of composites. The interlaminar bonding behavior of CF reinforced SMPNC was evaluated by peel tests. Fig. S2a shows the peel curve of a two-layer SMPNC specimen (200 mm × 20 mm) with a fully bonded interface. The peel force of the SMPNC remains around 11 N, corresponding to a peel strength of approximately 0.5 N/mm, indicating good interlaminar adhesion of the composite. Based on the specimen dimensions, the bonded area in the cutout region filled with SMPN prepolymer was designed to be 60%, 40%, and 20% of the specimen area, corresponding to 24 cm^2, 16 cm^2, and 8 cm^2, respectively. The peel test

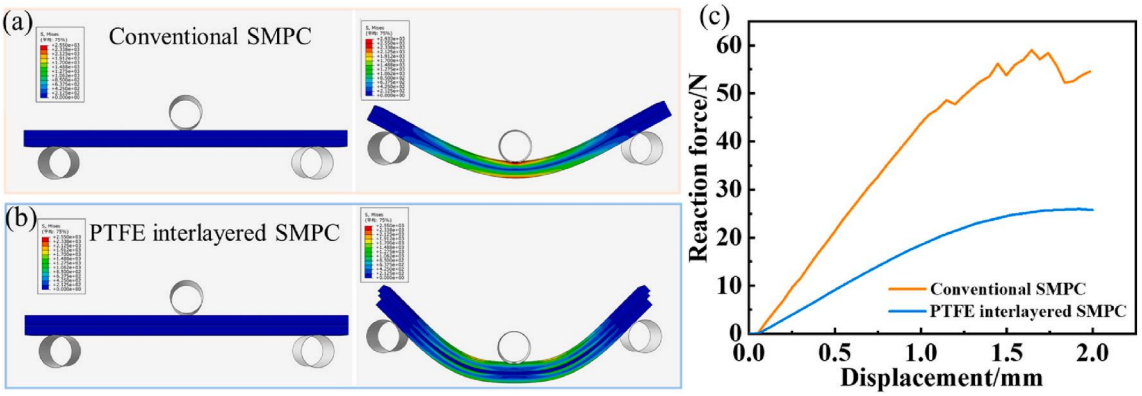

Fig. 2. Three-point bending simulated cloud diagrams of (a) conventional SMPC and (b) PTFE interlayered SMPC. (c) Reaction force-displacement curves at the loading nose from the simulated test.

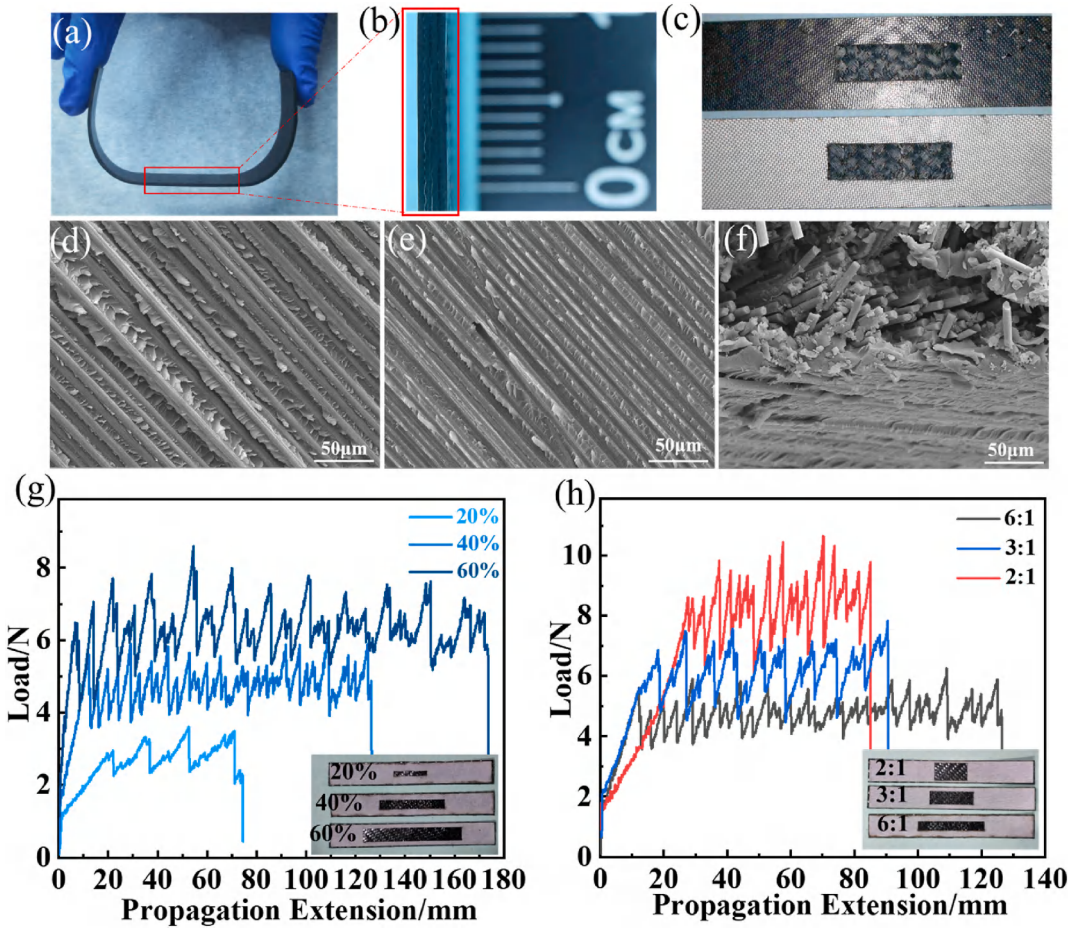

Fig. 3. (a) Digital image of SMPN-LC during bending at room temperature. (b) Side view of the interlaminar bonding region in SMPN-LC. (c) Macroscopic morphology of the interfacial bonding region after peeling. SEM images of (d-e) the bonding regions on both sides and (f) the cross-sectional of the interlayer. Peel curves of SMPN-LC (g) with different bonded area fractions and (h) with different length-width ratio.

results for these specimens are shown in Fig. 3g. As the bonded area decreases, the average peel force declines due to the reduced load-bearing interfacial width. Fig. S2b shows that while the peel strength remains constant around 0.55 N/mm, the peel force decreases with smaller bonded widths, as peeling is controlled by steady-state crack propagation, dependent on interfacial fracture toughness per unit width. Therefore, the interlayer bonded size has little impact on peel strength but affects peel force. Further investigation was conducted to evaluate the effect of length-width ratio on interfacial bonding performance. With the bonded area maintained at 40%, the length-width ratio of the cutout region in the PTFE interlayer was adjusted to 6:1, 3:1, and 2:1. Fig. 3h shows that increasing bonded width raises peel force, while reducing the bonded length limits the crack propagation, resulting in lower delamination displacement during peeling.

3.2. The mechanical test of SMPN-LC

To evaluate the mechanical properties of SMPN-LC, the SMPNC laminates without PTFE interlayers were tested as a reference. Three types of CF stacking SMPNC were prepared: 0/90° (0/90), ±45° (±45), and an interlayer alternating arrangement of 0/90° and ±45° (IA), with each SMPNC consisting of four CF plies. And the tensile and flexural performance of these SMPNCs is shown in Fig. S3a and Fig. S3b, respectively. The SMPNC of 0/90 exhibits the highest stiffness and strength, with an elastic modulus of 83 GPa and a tensile strength of 440 MPa, but the fracture strain is only 0.51%. The SMPNC of ±45 shows a higher fracture strain of 1.53%, while its tensile strength and stiffness are considerably reduced, with an elastic modulus of 27.8 GPa and a fracture stress of 140 MPa. The SMPNC of IA displays intermediate tensile properties, with an elastic modulus of 67.3 GPa, a fracture stress of 395 MPa. Overall, the tensile performance of IA falls between those of the 0/90° and ±45° configurations, which can be attributed to the synergistic contribution of piles with different orientations that promotes stress redistribution and coordinated deformation. A similar trend is observed in the bending results, where the bending strength and flexural modulus of IA SMPNC are intermediate between those of 0/90 and ± 45. Therefore, the interlayer alternating stacking arrangements, which provides relatively balanced mechanical properties, was adopted for fabricating SMPN-LC in the subsequent mechanical study.

Fig. 4a presents the tensile curves of SMPN-LC with different interlaminar bonded areas, and Fig. S4a summarizes the corresponding elastic modulus and tensile strength. As the interlaminar bonded area percentage decreases, the tensile strength drops from 379 MPa at 60% to 307 MPa at 20%. This decrease is attributed to the reduction in effective interlaminar bonding, which weakens load transfer across the interface and limits stress transmission between adjacent plies, thereby lowering the tensile strength of SMPN-LC. However, even when the interlaminar bonded area is reduced to 20%, the tensile strength remains as high as 307 MPa, indicating robust tensile performance of SMPN-LC. The flexural performance of SMPN-LC is shown in Fig. 4b, and the corresponding modulus and strength are presented in Fig. S4b. As the interlaminar bonded area fraction decreases from 60% to 20%, the flexural strength drops from 571 MPa to 426 MPa, accompanied by a reduction in flexural modulus from 34.6 GPa to 24.5 GPa, indicating weakened interlaminar stress transfer under bending. However, the fracture strain increases with decreasing interlaminar bonding area. This behavior is attributed

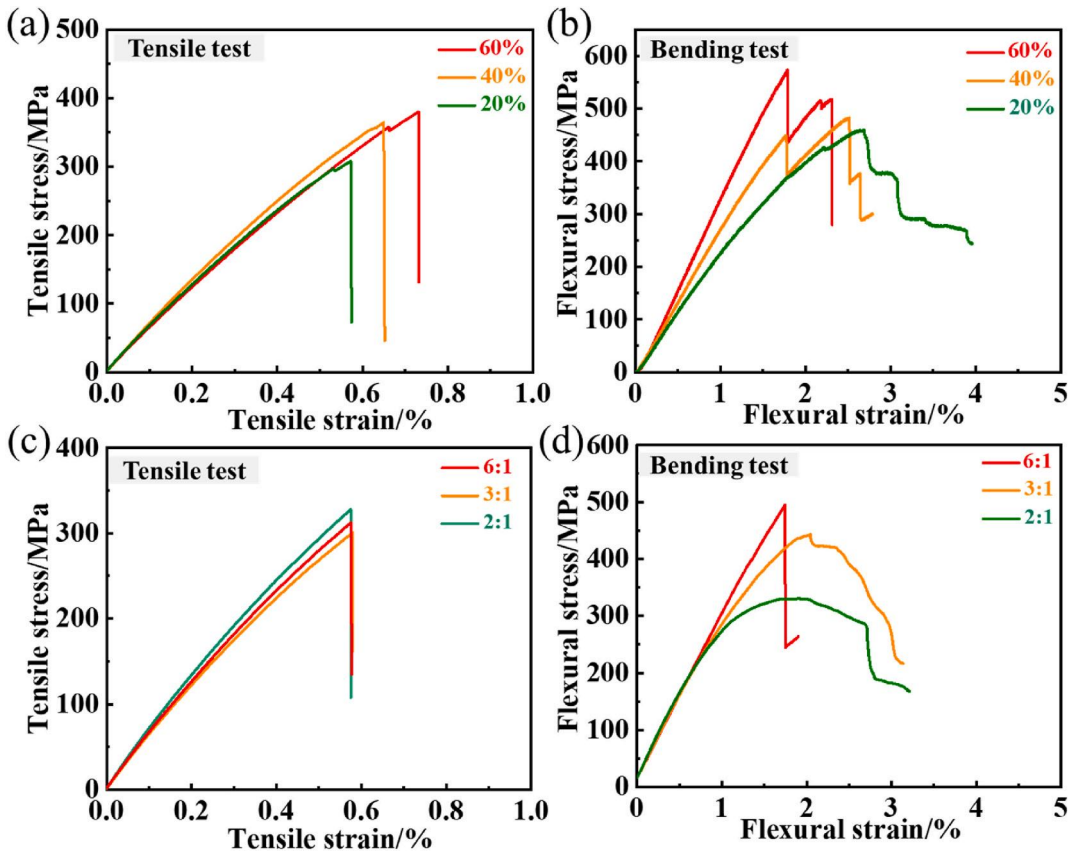

Fig. 4. (a) Tensile curves and (b) flexural curves of SMPN-LC with different bonded area fractions. (c) Tensile curves and (d) flexural curves of SMPN-LC at the 40% interlaminar bonded area with different length-width ratios.

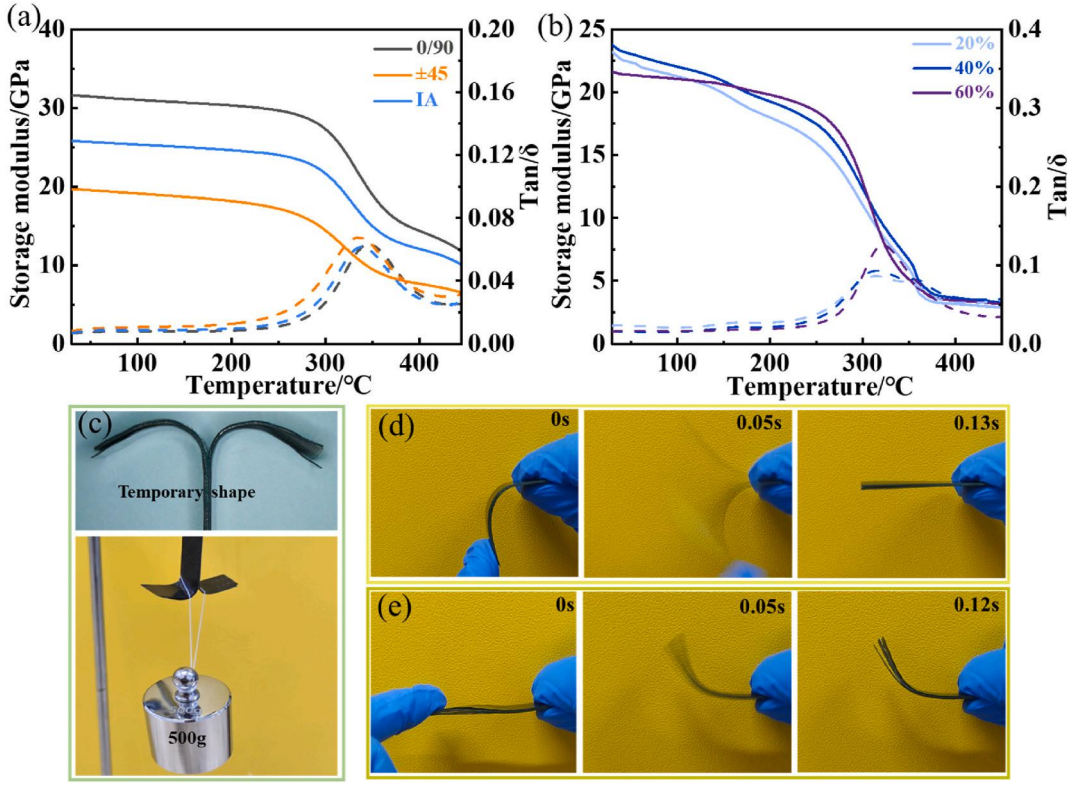

Fig. 5. (a) DMA curves of SMPNC with different CF fabrics stacking arrangements. (b) DMA curves of SMPN-LC with different bonded area fractions. (c) Temporary shape of SMPN-LC achieved via layer-wise deformation. Elastic recovery process of (d) SMPN-LC and (e) SMPN-LC in a temporary shape.

to the PTFE induced interlaminar decoupling of between adjacent SMPNC plies, which increases the extent of unbonded interfaces and activates interfacial slip during bending, thereby promoting stress redistribution and enhancing deformability.

The influence of the length-width ratio variation on the mechanical properties of SMPN-LC was further investigated. With the interlaminar bonded area maintained at 40%, Fig. 4c shows that the tensile properties of SMPN-LC remain almost constant across different length-width ratios. This is because the tensile properties are predominantly governed by the axial load-bearing capability of the CF within the SMPNC plies, and an identical interfacial bonded area provides comparable interlaminar load transfer, resulting in consistent tensile performance. Fig. 4d presents the flexural performance, and the corresponding modulus and strength are presented in Fig. S4d. The flexural modulus is insensitive to the length-width ratio and remains at approximately 30 GPa. The flexural strength decreases as the interlaminar bonded length is reduced, dropping from 493 MPa at 6:1 to 329 MPa at 2:1. This reduction is mainly associated with the shortened and widened bonding area, which constrains interlaminar load transfer and promotes local stress concentration, thereby leading to earlier failure in bending. However, a shorter bonded length increases the length of PTFE decoupling regions, providing a longer interfacial sliding path and improving deformation accommodation. Accordingly, the fracture strain increases from 1.8% at the length-width ratio of 6:1 to 2.9% at the ratio of 2:1. These results demonstrate that tailoring the interlaminar bonding geometry provides an effective route to tune the strength-ductility balance of SMPN-LC.

The dynamic mechanical behavior of SMPNC was characterized by DMA. Fig. 5a shows the DMA curves of SMPNC with different fabrics stacking arrangements. All specimens exhibit a similar glass transition temperature (T_g) of approximately 320 °C. This is because T_g is primarily determined by polymer segment mobility in the resin matrix and is insensitive to fabric arrangement. The storage modulus at room temperature is 32.0 GPa for the 0/90 SMPNC, 19.8 GPa for the ±45 SMPNC, and 25.4 GPa for the IA SMPNC, which is related to the fiber orientation and loading direction. After the glass transition, the storage modulus decreases rapidly but remains relatively high, which is beneficial for maintaining load-bearing capacity at high temperature. After PTFE decoupling, Fig. 5b shows that the variations in the interlaminar bonded area have little influence on the dynamic mechanical behavior of SMPN-LC, because the small oscillatory strain amplitude in DMA enables the bonded regions to carry the applied load and maintain strain continuity.

3.3. The shape memory behavior of SMPN-LC

The pronounced modulus contrast of SMPN-LC across the glass transition provides the mechanical basis for its shape memory behavior. As shown in Fig. S5a, a specimen weighing 4 g was deformed into a temporary bridge structure and can readily support a 200 g load, corresponding to 50 times its own weight, demonstrating reliable load-bearing capacity in the temporary shape. Upon thermal stimulation, the structure undergoes shape recovery, and the recovery process is illustrated in Fig. S5b. With the decoupling of PTFE, SMPN-LC exhibits stable shape fixation and recovery during repeated shape memory cycles. Fig. S6 demonstrates the stable temporary and recovered shapes observed in the 10th cycle. It is primarily attributed to the low surface energy of the PTFE layer, which weakens its interfacial bonding with the SMPN layer and provides an ultralow friction coefficient. These features facilitate interlayer slip and relieve stress concentrations during deformation, thereby mitigating mechanical damage and ensuring reliable deformation performance over repeated shape memory cycles.

Owing to the interlaminar isolation of PTFE, adjacent SMPNC plies in SMPN-LC are partially decoupled and can deform independently, allowing it to undergo layer-wise deformation. As shown in Fig. 5c, the specimen can be deformed into an anchor-hook structure capable of hanging a 500 g weight. This layer-wise deformation capability markedly expands the attainable shape diversity of shape memory composites.

In addition to its shape memory performance, the interlayer isolation of PTFE in SMPN-LC enables the decoupled regions to undergo elastic bending in the absence of interlaminar constraints. Fig. 5d shows that the decoupled regions of SMPN-LC can elastically bend to angles exceeding 90° at room temperature and rapidly recover within 0.13 s. Even after being deformed into a bent temporary shape, SMPN-LC still retains excellent elastic recoverability. As shown in Fig. 5e, when the bent temporary shape is flattened and then released, the structure quickly recovers to its temporary shape through elastic recovery within about 0.12 s. With the decoupling of PTFE, SMPN-LC maintains its shape memory performance while also exhibiting rapid elastic recovery property, thereby enhancing deformation adaptability and expanding structural design freedom.

3.4. The interface characterization of SMPN-LAC

Based on the PTFE interlayered design, incorporating functional interlayers into the SMPN-LC can further expand the application potential of the composite. Here, a thermally insulating SMPNA was introduced as an interlayer in SMPN-LC to fabricate SMPN-LAC, and the fabrication procedure is described in the experimental section. Fig. 6a presents a schematic of the interlayer structure of SMPN-LAC, and Fig. 6b shows photographs of the composites with different numbers of SMPNA layers. The internal morphology after peeling the surface SMPNC ply is shown in Fig. 6c, where residual SMPNA remains firmly adhered to the bonded regions. The interfacial bonding mechanism between SMPNC and SMPNA is illustrated in Fig. 6d. The PTFE cutout region was filled with SMPN prepolymer. During curing, the molten prepolymer infiltrates the microporous aerogel surface, forming mechanical interlocking at the SMPNA surface, thereby enhancing interlayer bonding stability. After curing, SMPNA and SMPNC exhibit good interfacial compatibility as they are derived from the same resin matrix. Fig. 6e shows the SEM micrograph of the bonding region in SMPN-LAC. From top to bottom, the interfacial layers consist of the SMPNA, SMPN/CNT bonding part, and SMPNC. The bonded thickness between SMPNA and SMPNC is approximately 130 μm, and the bonding between SMPN and SMPNA appears seamless, indicating good interfacial bonding quality.

The SMPN matrix endows both SMPNC ply and SMPNA layer with shape memory property, and the shape memory behavior of the SMPN-LAC is further demonstrated. The properties of SMPNA have been reported in our previous work [28], and Fig. S7 presents the shape recovery process of SMPNA. After being interlayered in SMPN-LC, the bending-recovery shape memory performance of SMPN-LAC is shown in Fig. 6f. The specimen is deformed into a bent temporary shape at 350 °C and fixed at room temperature. Upon reheating, it gradually recovers to its original shape. Actually, the PTFE interlayer plays a critical role during bending. By acting as a decoupling interlayer, PTFE alleviates the constraints imposed on SMPNA by adjacent SMPNC plies, thereby promoting interfacial sliding and enabling large bending deformation.

3.5. Thermal insulation performance of SMPN-LAC

The porous structure endows materials with excellent thermal insulation performance, and the thermal conductivity of SMPN-LAC with different numbers of SMPNA layers was measured using a Hot Disk thermal conductivity analyzer. Samples containing one, two, and three SMPNA layers were denoted as LAC-1, LAC-2, and LAC-3, respectively. And the test results are presented in Fig. 7a. The thermal conductivity of SMPN-LC in the thickness direction is 338.6 mW/m·K. After incorporating SMPNA layers, the conductivity decreased to 132.7 mW/m·K for LAC-1, 108.3 mW/m·K for LAC-2, and 104 mW/m·K for LAC-3, corresponding to a maximum reduction of 69% compared with SMPN-LC.

The thermal insulation performance for SMPN-LAC was evaluated by

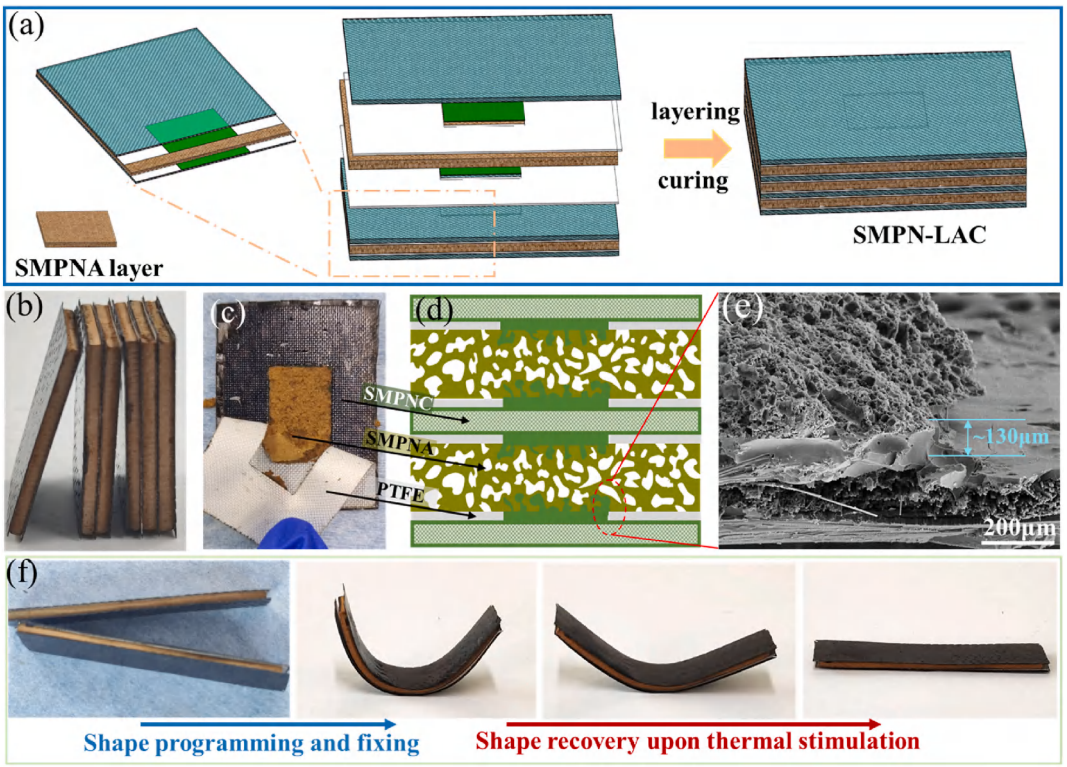

Fig. 6. (a) Schematic illustration of the SMPN-LAC interlaminar structure. (b) Digital image of SMPN-LAC with different numbers of SMPNA layer. (c) Macroscopic morphology of the interfacial bonding region after peeling. (d) Interfacial bonding illustration of SMPN-LAC. (e) SEM images of the bonded interfaces. (f) Bending-recovery shape memory process of SMPN-LAC.

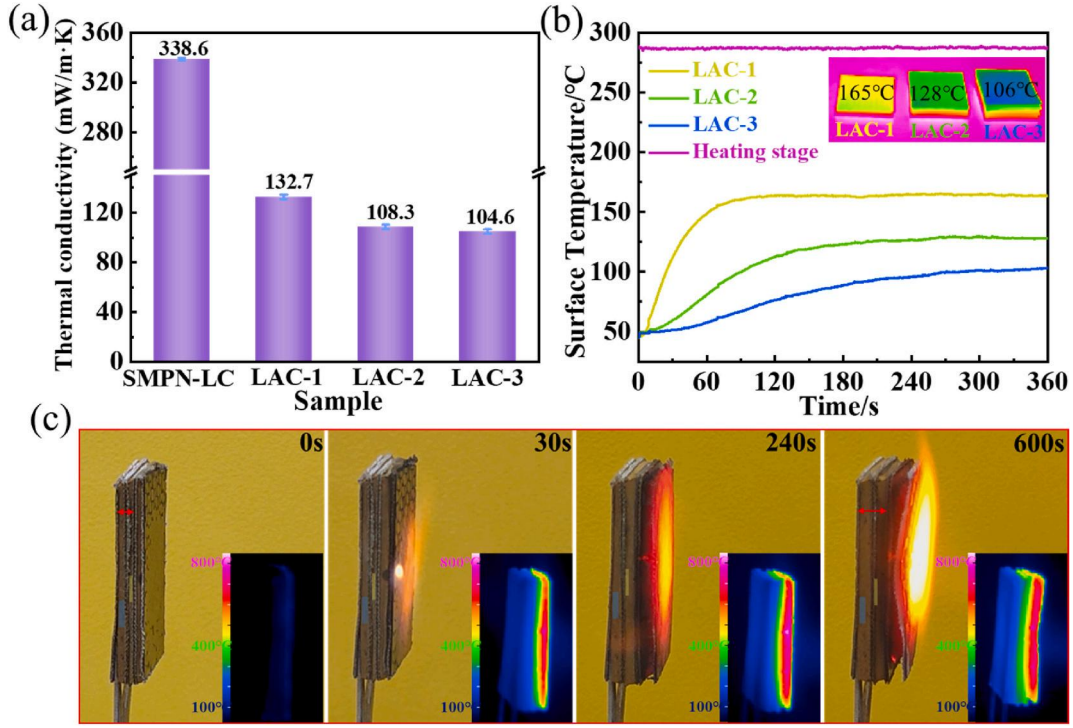

Fig. 7. (a) Thermal conductivity of SMPN-LAC. (b) Time-dependent temperature curves of SMPN-LAC on the heating stage of 300 °C. (c) Thermal protection process of SMPN-LAC in a compressed temporary shape under butane flame.

placing the samples on a heated stage at temperature of 300 °C, and Fig. 7b presents the corresponding time-dependent surface temperature curves. The upper surface temperature of LAC-1 stabilized at approximately 165 °C after 60 s. As the number of SMPNA layers increased, the temperature of LAC-2 reached about 128 °C at around 120 s, and LAC-3 stabilized at about 106 °C after 240 s. Although the

increased thickness of SMPN-LAC contributes to lowering the heat transfer rate, the alternating stacking of SMPNC and SMPNA further induces repeated interfacial heat flux interruption and redistribution. These interfacial disruptions promote a more dispersed heat transfer pathway, thereby reducing the heating rate. SMPN is a SMP with a high glass transition temperature, excellent thermal stability, and ablation resistance, making it particularly suitable for thermally triggered applications in high temperature environments [27]. With SMPNA incorporate in to SMPN-LC, the enhanced thermal insulation of SMPN-LAC slows down heat transfer, thereby delaying shape recovery and limiting its applicability in scenarios requiring rapid actuation. However, this characteristic becomes advantageous in applications that require controllable or gradual actuation, such as thermal protection systems and deployable buffering structures. Owing to the combination of low thermal conductivity and thermally responsive shape memory behavior, SMPN-LAC shows great potential for use in smart thermal protection systems.

The thermal protection performance of SMPN-LAC was evaluated by butane flame (~1100 °C). Fig. S8a shows the photograph and infrared thermograph of SMPN-LAC after 300 s of flame exposure, and Fig. S8b presents the corresponding temperature evolution of each SMPNA layer. After 300 s, the temperature of the first SMPNA layer reached approximately 400 °C, while it decreased to about 200 °C at the second SMPNA layer and around 100 °C at the third layer. This attenuation is attributed to interfacial heat spreading between layers and the thermal insulation of SMPNA, indicating the strong potential of SMPN-LAC for thermal protection applications. In addition to the thermal insulation performance, the porous SMPNA also enables SMPN-LAC to possess compression-recovery shape memory property. Fig. S9a presents the thickness of SMPN-LAC before and after deformation, and Fig. S9b shows the shape recovery process. After shape fixation, the thickness of SMPN-LAC decreased from 3.44 mm (original) to 2.16 mm (temporary), corresponding to a compressive strain of 37% and a shape fixity ratio of 99%. With thermal stimulation, the compressed SMPN-LAC gradually recovered, stabilized at 3.16 mm, which presents a shape recovery ratio of approximately 78%.

Based on its compressive shape memory performance, SMPN-LAC provide graded thermal protection under high temperature. Fig. 7c shows a SMPN-LAC containing three SMPNA layers, deformed into a compressed temporary shape and exposed to a butane flame, with corresponding infrared thermographs inset. As heating proceeded, the SMPNA layers underwent sequential shape recovery, as shown in the Supporting Video 1. Within 30 s, the surface temperature of the first SMPNA layer reached 600 °C, triggering its shape recovery, while the porous SMPNA insulation maintained the second and third SMPNA layers below 300 °C, allowing them to retain their compressed shapes. After 240 s, the first SMPNA layer reached nearly 800 °C and oxidized. Meanwhile, the surface temperature of the second SMPNA layer increase to about 500 °C, triggering its shape recovery. With continued flame exposure, heat transfer remained slow owing to the ablation resistance of the SMPNC ply and the thermal insulation provided by SMPNA. After 600 s of butane flame exposure, the third SMPNA layer completes shape recovery, while the opposite-side temperature remained around 300 °C, demonstrating effective thermal protection of SMPN-LAC.

By combining the bending-recovery and compression-recovery shape memory properties, SMPN-LAC can simultaneously present shape memory behavior in two dimensions. Fig. 8a shows the shape recovery process of the temporary shape of SMPN-LAC after compression and bending deformation under a butane flame, and specific shape recovery details and thermal information are provided in Supporting Video 2 and 3. With the thermal stimulation of butane flame, SMPN-LAC gradually recovered from its bent and compressed temporary shape to its original shape. During the continuous heating process, the back temperature of SMPN-LAC remained below 400 °C, and heat diffusion to the surroundings was suppressed.

Supplementary data related to this article can be found online at https://doi.org/10.1016/j.coco.2026.102823

Fig. 8b further elucidates the thermal protection mechanism of SMPN-LAC. Through programming, SMPN-LAC is deformed into a temporary shape in which the pores of the interlayer SMPNA are compressed. The temporary shape remains stable below 300 °C (the deformation temperature). When SMPN-LAC is exposed to high temperature heat flux, the CF in the SMPNC plies promote in-plane heat spreading and redistribution, and the porous SMPNA provides thermal insulation

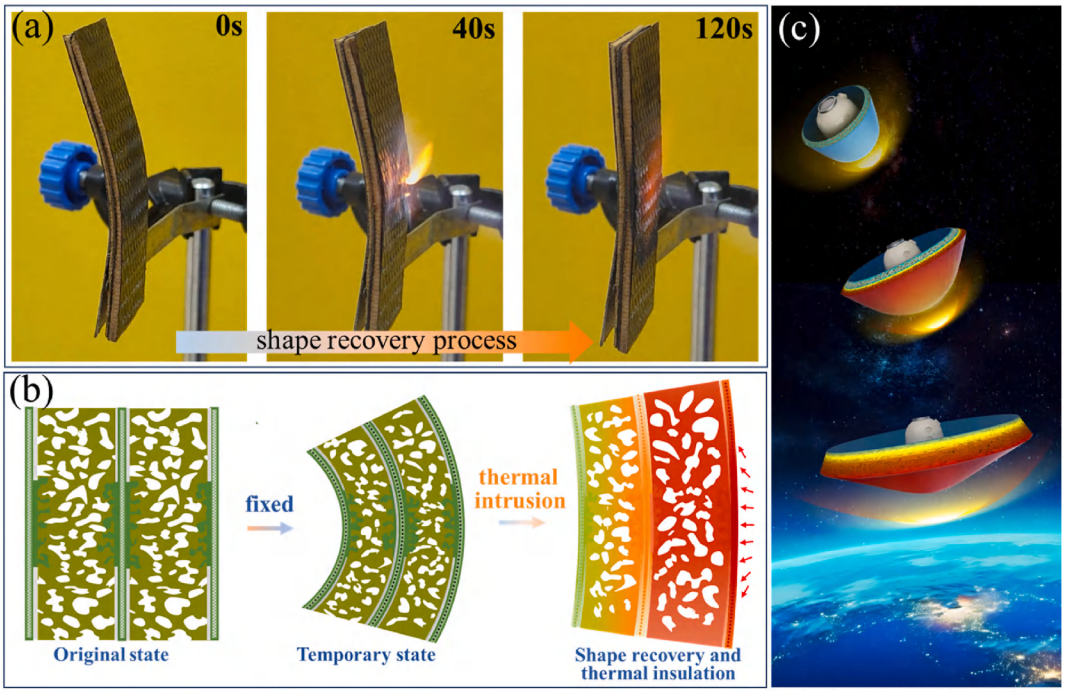

Fig. 8. (a) The shape recovery process of the bent and compressed temporary shape of SMPN-LAC. (b) Illustration of the thermal protection mechanism of SMPN-LAC. (c) Schematic of SMPN-LAC serve as the thermal shield for spacecraft.

across the thickness. Once the temperature exceeds 300 °C, the SMPNC ply and SMPNA layer are thermally triggered and recover toward original shape. The reopening of the pore structure in SMPNA reduces the effective thermal conductivity and lengthens the heat transfer path, hindering heat transfer in both the thickness and in-plane directions. When the incoming heat reaches the inner SMPNC plies, interfacial thermal resistance together with in-plane heat spreading within SMPNC markedly reduces the heat delivered to the next SMPNA layer, resulting in a lower temperature at that layer. In this way, high temperature heat flux triggers shape recovery in SMPNA, which increases the heat transfer path length, and the heat redistribution at the SMPNA/SMPNC interfaces reinforces the interfacial thermal barriers. Hence, through the shape memory performance and layer-by-layer thermal barrier structure, multilevel deformation regulated thermal protection is realized in SMPN-LAC.

Benefiting from its shape memory and thermal insulation properties, SMPN-LAC possesses great potential for smart thermal protection. Fig. 8c presents a schematic of SMPN-LAC serving as the thermal shield for spacecraft. When the spacecraft experiences high-speed friction with the atmosphere, the bending recovery of SMPN-LAC is triggered by frictional heat, deploying the shield and enhancing the spacecraft's aerodynamic deceleration. Meanwhile, the compression recovery of SMPN-LAC improves the thermal insulation of the shield, protecting the spacecraft from high temperatures. The shape memory behavior in two dimensions makes SMPN-LAC a promising material for advanced thermal protection systems.

4. Conclusion

In this work, a PTFE interlayer strategy was developed to decouple adjacent SMPNC plies, thereby enhancing the bending deformability of the SMPN-LC. Mechanical testing shows that the interlaminar bonded area had a negligible influence on the tensile modulus of SMPN-LC. With the interlayer-alternating layup of ±45° and 0/90° CF, the tensile modulus remained stable at around 60 GPa. The tensile strength depended strongly on the interlaminar bonded area, decreasing from 379 MPa to 307 MPa as the bonded area was reduced from 60% to 20%. Under bending, both flexural strength and flexural modulus decreased with decreasing interlaminar bonded area. At a bonded area of 20%, SMPN-LC retained a flexural strength of 426 MPa and a flexural modulus of 24.5 GPa. Under the same bonded area, shorter bonded lengths resulted in higher attainable bending strain. This behavior is mainly attributed to the PTFE enabled interlaminar decoupling, which activates interlaminar sliding and alleviates local stress concentrations during bending. With PTFE interlayers acting as decoupling layers, SMPN-LC exhibits layer-wise shape memory behavior, which enhances its deformation adaptability and structural design freedom for shape memory applications. With the further introduction of SMPNA, the thermal conductivity of SMPN-LAC decreases to 104 mW/m·K, and demonstrate good thermal insulation performance. Under thermal stimulation, SMPN-LAC exhibits both bending and compressive shape memory behavior. In the compressed temporary shape, the SMPNA in SMPN-LAC recovers gradually to form layer-by-layer thermal barrier, with the opposite-side temperature remaining at around 300 °C after 600 s of butane flame exposure. The proposed interlayer strategy integrates SMPNA layers between SMPNC plies, significantly enhancing the thermal insulation performance of the composites and thereby broadening the application potential of SMPCs in smart thermal protection systems.

CRediT authorship contribution statement

Rongxiang Hu: Investigation, Writing – original draft. **Fenghua Zhang:** Funding acquisition, Writing – review & editing. **Yanju Liu:** Funding acquisition. **Jinsong Leng:** Resources, Supervision.

Declaration of competing interest

The authors declare that they have no known competing financial interests or personal relationships that could have appeared to influence the work reported in this paper.

Acknowledgements

This work was financially supported by the National Natural Science Foundation of China (Grant No. 92271112 and No.92271206).

Appendix A. Supplementary data

Supplementary data to this article can be found online at https://doi.org/10.1016/j.coco.2026.102823.

Data availability

Data will be made available on request.

References

[1] R. Zende, V. Ghase, V. Jamdar, A review on shape memory polymers, Polymer-Plastics Technol. Mater. 62 (4) (2023) 467–485, https://doi.org/10.1080/25740881.2022.2121216.
[2] S.K. Chandaka, A. Das, P. Laskar, Emergence of shape memory polymers as a new material for diverse applications, RSC Adv. 15 (38) (2025) 31210–31229, https://doi.org/10.1039/d5ra04372g.
[3] W. Liu, W. Zhao, K.R. Xie, X.F. Li, Y.F. Wang, D.Y. Kong, Y.J. Liu, J.S. Leng, Toughening and responsive contractile shape memory fibrous membrane via water for mechanically active wound dressing, Adv. Fiber Mater. 6 (6) (2024) 1942–1954, https://doi.org/10.1007/s42765-024-00463-z.
[4] J. Zou, Y.Z. Wang, X. Yu, R.L. Liu, W.Q. Fan, J. Cheng, W.Y. Cai, Skin-Inspired Zero carbon heat-moisture management based on shape memory smart fabric, Adv. Fiber Mater. 7 (2) (2025) 481–500, https://doi.org/10.1007/s42765-024-00496-4.
[5] B.T. Lu, E.L. Hu, W.W. Ding, W.Y. Wang, R.Q. Xie, K. Yu, F. Lu, G.Q. Lan, F.Y. Dai, Bioinspired hemostatic strategy via pulse ejections for severe bleeding, Wounds, Research 6 (2023), https://doi.org/10.34133/research.0150.
[6] L. Luo, F.H. Zhang, L.L. Wang, Y.J. Liu, J.S. Leng, Recent advances in shape memory polymers: multifunctional materials, multiscale structures, and applications, Adv. Funct. Mater. 34 (14) (2024), https://doi.org/10.1002/adfm.202312036.
[7] Y.K. Liu, L.L. Wang, Y.J. Liu, F.H. Zhang, J.S. Leng, Recent progress in shape memory polymer composites: driving modes, forming technologies, and applications, Compos. Commun. 51 (2024), https://doi.org/10.1016/j.coco.2024.102062.
[8] C.P. Kumar, N. Sivanagaraju, D. Loknath, G.N.M. Rao, M.R.K. Vakkalagadda, Shape memory polymers, blends, and composites: processing, properties, and applications, Polymer-Plastics Technology and Materials 64 (9) (2025) 1253–1281, https://doi.org/10.1080/25740881.2025.2460063.
[9] K. Yadav, A. Singhwane, M. Milli, N. Gorhe, A.K. Srivastava, S. Verma, Shape memory polymers as new advanced loss circulation materials for drilling applications, Polym. Bull. 81 (17) (2024) 15293–15317, https://doi.org/10.1007/s00289-024-05342-6.
[10] X. Wan, S.Y. Chen, J.Q. Ma, C.Q. Dong, H. Banerjee, S. Laperrousaz, P.L. Piveteau, Y. Meng, J.S. Leng, F. Sorin, Multimaterial shape memory polymer fibers for advanced drug release applications, Adv. Fiber Mater. 7 (5) (2025) 1576–1589, https://doi.org/10.1007/s42765-025-00571-4.
[11] Q.B. Peng, S. Wang, J.G. Han, C.Y. Huang, H.Y. Yu, D. Li, M. Qiu, S. Cheng, C. Wu, M.X. Cai, S.X. Fu, B.H. Chen, X.Y. Wu, S.W. Du, T.T. Xu, Thermal and magnetic dual-responsive catheter-assisted shape memory microrobots for multistage vascular embolization, Research 7 (2024), https://doi.org/10.34133/research.0339.
[12] B.B. Du, X.Y. Zhang, T. Wang, Y.F. He, M.Y. Shen, T. Yu, Three-Dimensional printable color-modulation and shape-programmable structures: an encryption key for image, Recognition Electronic Locks, Research 8 (2025), https://doi.org/10.34133/research.0666.
[13] G.Q. Ming, F.F. Li, M.M. Xu, C.J. Zeng, W. Zhao, L.W. Liu, Y.J. Liu, J.S. Leng, Shape memory cyclic behavior and mechanical durability of woven fabric reinforced shape memory polymer composites, Compos. Sci. Technol. 258 (2024), https://doi.org/10.1016/j.compscitech.2024.110866.
[14] Z.H. Li, W.Q. Du, Y. Liu, Y.W. Ouyang, Shape memory properties of mirror-symmetric weft Plain knitted fabric-reinforced polymer composites under tensile and U-Bending loads, Fibers Polym. (2025), https://doi.org/10.1007/s12221-025-01282-8.
[15] H.P. Ren, Y.W. Ouyang, S.L. Xiao, W.L. Xu, Y. Liu, Shape memory property and mechanism of the knitting-fabric reinforced epoxy composites subjected to tensile loading, Compos. Sci. Technol. 230 (2022), https://doi.org/10.1016/j.compscitech.2022.109764.

[16] K. Shahi, V. Ramachandran, R. Mohan, B. Ramachandran, Shape memory properties of short-glass fiber reinforced epoxy composite programmed below glass transition temperature, J. Polym. Mater. 42 (2) (2025) 477–496, https://doi.org/10.32604/jpm.2025.062481.
[17] A. Hassan, H. Dahy, Tailored continuous flax fiber-reinforced shape memory polymer biocomposites: enhanced thermomechanical and shape memory performance for sustainable structural applications, Compos. B Eng. 307 (2025), https://doi.org/10.1016/j.compositesb.2025.112840.
[18] A. Yadav, S.K. Singh, S. Das, S. Kumar, A. Kumar, Shape memory polymer and composites for space applications: a review, Polym. Compos. 46 (13) (2025) 11647–11683, https://doi.org/10.1002/pc.29707.
[19] Z.H. Li, Y. Yang, L. Ma, H.X. Liu, X. Zhang, Shape memory epoxy resin and its composite with good shape memory performance and high mechanical strength, Polym. Bull. 80 (2) (2023) 1641–1655, https://doi.org/10.1007/s00289-022-04140-2.
[20] B. Tatár, L. Mészáros, Shape memory effect in cross-linked polyethylene matrix composites: the effect of the type of reinforcing fiber, Polym. Bull. 81 (7) (2024) 6311–6323, https://doi.org/10.1007/s00289-023-05003-0.
[21] C.J. Zeng, L.W. Liu, Y. Du, M. Yu, X.Z. Xin, P.L. Xu, F.F. Li, L.L. Wang, F.H. Zhang, Y.J. Liu, J.S. Leng, Space-deployable device based on shape memory cyanate ester composites, Compos. Commun. 42 (2023).
[22] Y. Li, F. Zhang, Y. Liu, J. Leng, Programmable shape memory bismaleimide composite claw with two-way grabbing function, Compos. Appl. Sci. Manuf. 165 (2023), https://doi.org/10.1016/j.compositesa.2022.107328.
[23] R. Belliveau, B. Landry, G. LaPlante, Comparative study of the mechanical properties of woven and unidirectional fibres in discontinuous long-fibre composites, J. Thermoplast. Compos. Mater. 36 (6) (2023) 2372–2389, https://doi.org/10.1177/08927057221091084.
[24] Y.Y. Chang, W.B. Young, Study on the characteristics of vacuum-bag-only processed composites by prepreg/fiber interleaved layup, Fibers Polym. 24 (2) (2023) 653–670, https://doi.org/10.1007/s12221-023-00026-w.
[25] Y.H. Xiang, Z.W. Zhang, X.N. Yang, Y. Lin, G.K. Zhang, M.Q. Sun, F.G. Yan, M. Y. Wang, Failure mechanism of carbon/ultra-high molecular weight polyethylene twill fiber reinforced hybrid laminates under ballistic impact, Mater. Des. 216 (2022), https://doi.org/10.1016/j.matdes.2022.110578.
[26] A.N.S. Boztas, A.E. Atespare, D. Serttan, M. Yildiz, S. Unal, B. Dizman, Optimizing the cure cycle of aerospace-grade carbon fiber-reinforced epoxy composites through comparative analysis of resin and prepreg cure kinetics, Polym. Compos. 46 (18) (2025) 16724–16737, https://doi.org/10.1002/pc.70067.
[27] R.X. Hu, F.H. Zhang, L. Luo, L.L. Wang, Y.J. Liu, J.S. Leng, An end-capping strategy for shape memory phthalonitrile resins via annealing enables conductivity and wave-absorption, Chem. Eng. J. 489 (2024), https://doi.org/10.1016/j.cej.2024.150956.
[28] R.X. Hu, F.H. Zhang, L. Luo, L.L. Wang, Y.J. Liu, J.S. Leng, Reconfigurable high-temperature thermal protection shape memory aerogel based on phthalonitrile resin with facile template method, Carbon 242 (2025), https://doi.org/10.1016/j.carbon.2025.120378.